ABSTRACT

INVESTIGATION OF DOUBLE RESONANCE SPECTROSCOPY OF IODINE MOLECULES
FOR USE IN QUANTUM BEAT EXPERIMENTS

by Corey McDonald

The resonant $B^3\Pi_u^+ \leftarrow X0_g^+$ and resonant $E0_g^+,D'2_g \leftarrow B^3\Pi_u^+ \leftarrow X0_g^+$ transitions of $I_2$ vapor have been studied by direct observation of fluorescence emitted from the B, E and D$'$ states, respectively. Potential energy curves for the $X0_g^+$, $B^3\Pi_u^+$, $D0_u^+$, $D'2_g$, $A'2_u$ and $E0_g^+$ states are calculated using Dunham coefficients from literature via the Rydberg-Klein-Rees Inversion Method. The generated turning points are then used to calculate Franck-Condon factors and Einstein A-coefficients. Both one and two-photon emission spectra are observed and analyzed.

# INVESTIGATION OF DOUBLE RESONANCE SPECTROSCOPY OF IODINE MOLECULES FOR USE IN QUANTUM BEAT EXPERIMENTS

A thesis submitted to

the Miami University Honors Program

in partial fulfillment of the

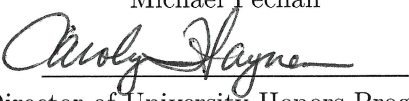requirements for

University Honors with Distinction

by

Corey McDonald

Miami University

Department of Physics

Oxford, Ohio

April 2012

Advisor_____
Burcin S. Bayram

Reader_____
Burcin Bayram

Reader_____
Michael Pechan

_____
Director of University Honors Program,
Carolyn A. Haynes

# Contents

# List of Tables

# List of Figures

## ACKNOWLEDGMENTS

# Chapter 1

# Introduction

## 1.1 Introduction

We have measured the two-photon double resonance excitation spectrum of molecular iodine by using pulsed pump and probe lasers. In the experiment, the pump laser is exciting the B-X transition at 532 nm while the probe laser is exciting the D$'$-B or E-B transitions at 438.26 nm. By achieving two-photon excitation of the D$'$ or E states, we have demonstrated the viability of using this excitation pathway for use in a study of quantum beats in molecular iodine. In addition, the D$'$ and E fluorescence obtained can be used to extract Dunham coefficients and electric dipole moment transition functions. A brief overview of Dunham expansion, the RKR inversion method, Franck-Condon factors, Einstein A-coefficients, the thermal distribution of rotational levels in diatomic molecules, and quantum beats is also given.

## 1.2 Motivation

Broadening effects such as Doppler and power broadening can obscure spectral features and compromise the accuracy of measured spectra. An effective way of eliminating Doppler broadening effects is by using quantum beat spectroscopy. Quantum beats can be generated by exciting a molecule to a coherent superposition of closely-lying non-degenerate energy eigenstates, such as rotational levels. When a single level is excited, the fluorescence from this decay appears as an decaying exponential. When a superposition of multiple coherently-excited levels decay, the fluorescence intensity has an oscillatory modulation that results from quantum interference of the wavefunctions of the two states. The beat frequency is dependent upon the energies of the excited states. Applying a Fourier Transform to the time-dependent fluorescence yields a Doppler-free spectrum of the ro-vibrational levels, allowing for a high-precision measurement of spectral features. The rotational lines of diatomic molecules have energy differences on the order of 1 cm$^{-1}$. To avoid making several transitions with a single, relatively broadband pump laser, one can use a narrow bandwidth laser to excite a single rovibrational level. Then, a second laser with a sufficiently broad bandwidth can be used to excite the molecule into a coherent superposition of states from which to observe quantum beats. A good candidate for the first laser is a continuous-wave laser, especially a diode laser, as these types of lasers typically have a very narrow bandwidth. Diode lasers in particular can be very slightly tuned by adjusting current and temperature. For the second laser, a pulsed dye laser in a Littrow configuration would likely have the necessary bandwidth.

The purpose of this experiment is to determine a pathway in molecular iodine to be used in a quantum beat spectroscopy experiment to determine the spectroscopic parameters of the D′, and possibly E, electronic states. The high-resolution, Doppler-free spectra obtained from using the quantum beat technique is necessary for gaining precise measurements. Although the B and X electronic levels of iodine have been studied in considerable detail, data on the upper levels remains sparse and inconsistent in contemporary literature [1, 3, 4].

## 1.3 Structure of Diatomic Molecules

The spectra of diatomic molecules are distinctly different from that of single atoms. Whereas single atoms possess single energy levels with nearly-degenerate hyperfine levels, molecules have electronic energy levels, with many vibrational levels for each, and many rotational levels for each vibrational level. The electronic levels of a molecule are a result of the different electronic states of the atoms it is composed of. A diatomic molecule is often modeled as two atoms connected by an electromagnetic spring, and as the system can vibrate and rotate, energy can be stored in these modes, which gives rise to the vibrational and rotational energy states. The electronic states form potential energy wells, within which the rovibrational eigenfunctions form.

The notation for the electronic states in diatomic molecules is similar to notation for single atoms, and merits some explanation. In general, a state is labeled $^{2S+1}\Lambda^{\pm}_{\Omega,(u/g)}$. S is the total spin quantum number, $\Lambda$ is the projection of the orbital angular momentum along the internuclear axis, $\Omega$ is the projection of the total angular momentum along the internuclear axis, u/g denotes the parity of the wavefunction, and $\pm$ describes the reflection symmetry along a plane containing the internuclear axis. The parity described by u/g is determined as follows: consider the center of mass of the molecule to be the origin along the internuclear axis. If reflecting the positions of the electrons in a state over the origin leaves the wavefunction unchanged, then it is called a gerade state and is labeled with g. If it inverts the wavefunctions, it is called ungerade and is labeled u. The $\pm$ parity is determined by the symmetry of the wavefunction across a plane that contains the internuclear axis. If the wavefunction is symmetric across the plane, the state is labeled as +, if it is antisymmetric, the state is labeled as -. The different values of $\Lambda$ have traditional symbols associated with them: $\Lambda = 0, 1, 2, 3$ are denoted by $\Sigma, \Pi, \Delta$, and $\Phi$, respectively [6].

# Chapter 2

# Theory

## 2.1 Optical Transitions in Molecules

For low-lying vibrational levels in the $I_2$ molecule, the vibrational energies are separated by about 200 cm$^{-1}$ in the X state, and by about 120 cm$^{-1}$ in the B state. Low-lying rotational energies are separated by about 3 cm$^{-1}$. At room temperature, the thermal energy $k_B T \approx hc/\lambda$ corresponds to $1/\lambda \approx 200$ cm$^{-1}$ = 6 THz. Therefore, only low-lying v''=0,1,2,3 vibrational states are populated with up to about a hundred rotational states. Due to symmetries and the resulting conservation laws, not all transitions are allowed. The allowed transitions obey selection rules [7], which are given by the Table 2.1.

Table 2.1: Selection Rules for an Electric Dipole Allowed Transition in Molecules.

| $\Delta\Lambda$ | $=$ | 0, 1 | |
|---|---|---|---|
| gerade (g) | $\leftrightarrow$ | ungerade (u) | |
| $\Delta J \equiv J' - J''$ | $=$ | -1 (P Branch) | |
| | $=$ | 0 (Q Branch) | but not J'=0 $\leftrightarrow$ J''=0 |
| | $=$ | +1 ( R Branch) | |

There is no strict selection rule for the change $\Delta$v in vibrational quantum number during an electronic transition. Thus, sequences of transitions can be observed. The selection rules for electronic transitions are based on conservation of angular momentum and on the Franck-Condon principle which governs which vibrational states can be accessed. Thus, we must turn to the Franck-Condon principle to understand which vibronic transitions we expect to excite. Franck-Condon principle is also based on the fact that electrons are much lighter than nuclei. For example, the electron redistribution which results from an electronic transition occurs instantaneously with respect to the nuclear motion. That is, the nuclei do not move during a transition. Transitions of the highest intensities occur when the overlap between the ground and excited state wavefunctions is largest.

## 2.2 Dunham Expansion Theory

The most commonly-used expression for calculating the energy of rovibronic states is the Dunham expansion. It is a power series expansion of the generalized potential of a rotating, vibrating molecule which contains vibrational and rotational contributions to the total energy, as well as their

cross terms. The Dunham theory is an improvement on an older model based on Morse potentials, which disagrees with experiment at higher vibrational and rotational energy levels. The formula is given by

$$E_{v,J} = \sum_{n,k} Y_{n,k}(v + \frac{1}{2})^n J^k (J+1)^k. \tag{2.1}$$

The $(v + \frac{1}{2})$ terms are a result of modeling the potential as a classical harmonic oscillator, where the particle in a potential well has a zero energy [8]. This gives a more general formula than the traditional expansion,

$$E_{v,J} = T_e + G(v) + B_v J(J+1) - D_v J^2 (J+1)^2, \tag{2.2}$$

where G(v) is the vibrational energy, $B_v$ is the rotational constant for the $v^{th}$ vibrational level, and $D_v$ is the centrifugal distortion constant for the $v^{th}$ vibrational level. $B_v$ and $D_v$ have their own expansions:

$$B_v = B_e - \alpha_e(v + \frac{1}{2}) + \dots \tag{2.3a}$$

$$D_v = D_e - \beta_e(v + \frac{1}{2}) + \dots \tag{2.3b}$$

Although these are sufficient for low vibrational and rotational levels, their accuracy becomes unreliable as v and J increase. Thus, the Dunham expansion is more favorable [7].

## 2.3 Determination of Molecular Potentials

### 2.3.1 RKR Calculations for Turning Points of Electronic Potentials

The transitions we select are based on calculated Franck Condon Factors (FCF). FCFs can also be used to calculate the relative intensities of peaks in the emission spectrum. These FCFs are calculated from potentials generated using the Rydberg-Klein-Rees (RKR) Inversion Method, which uses experimentally-determined values of Dunham coefficients and the dipole moment functions for each transition. This remarkable procedure is based upon a semi-classical approximation for the motion of the nuclei. The main part of the RKR method involves evaluating the following integrals [9, 10, 11]:

$$r_2(v) - r_1(v) = \sqrt{\frac{C_u}{\mu}} \int_{v_{min}}^{v} \frac{dv'}{[G_v - G_{v'}]^{1/2}} = f, \qquad (2.4a)$$

$$\frac{1}{r_2(v)} - \frac{1}{r_1(v)} = \sqrt{\frac{\mu}{C_u}} \int_{v_{min}}^{v} \frac{B_{v'}dv'}{[G_v - G_{v'}]^{1/2}} = g, \qquad (2.4b)$$

where $r_1$ and $r_2$ are the inner and outer turning points of the potential, respectively, $v_{min}$ is the effective vibrational quantum number value at the potential minimum (typically $-\frac{1}{2}$), $\mu$ is the reduced mass of the molecule, and $C_u = \frac{\hbar^2}{2}$. Equations (2.4a) and (2.4b) can be rearranged to yield

$$r_1(v) = \sqrt{f^2 + \frac{f}{g}} - f, \qquad (2.5a)$$

$$r_2(v) = \sqrt{f^2 + \frac{f}{g}} + f. \qquad (2.5b)$$

The Fig. 2.1 shows our calculated plots of RKR curves for $I_2$ X, A', B, D, D', and E states. Note that the A' potential turning points were taken from Ref. [4]. Thus, we have taken the RKR values for the A' state to plot the potential energy curve.
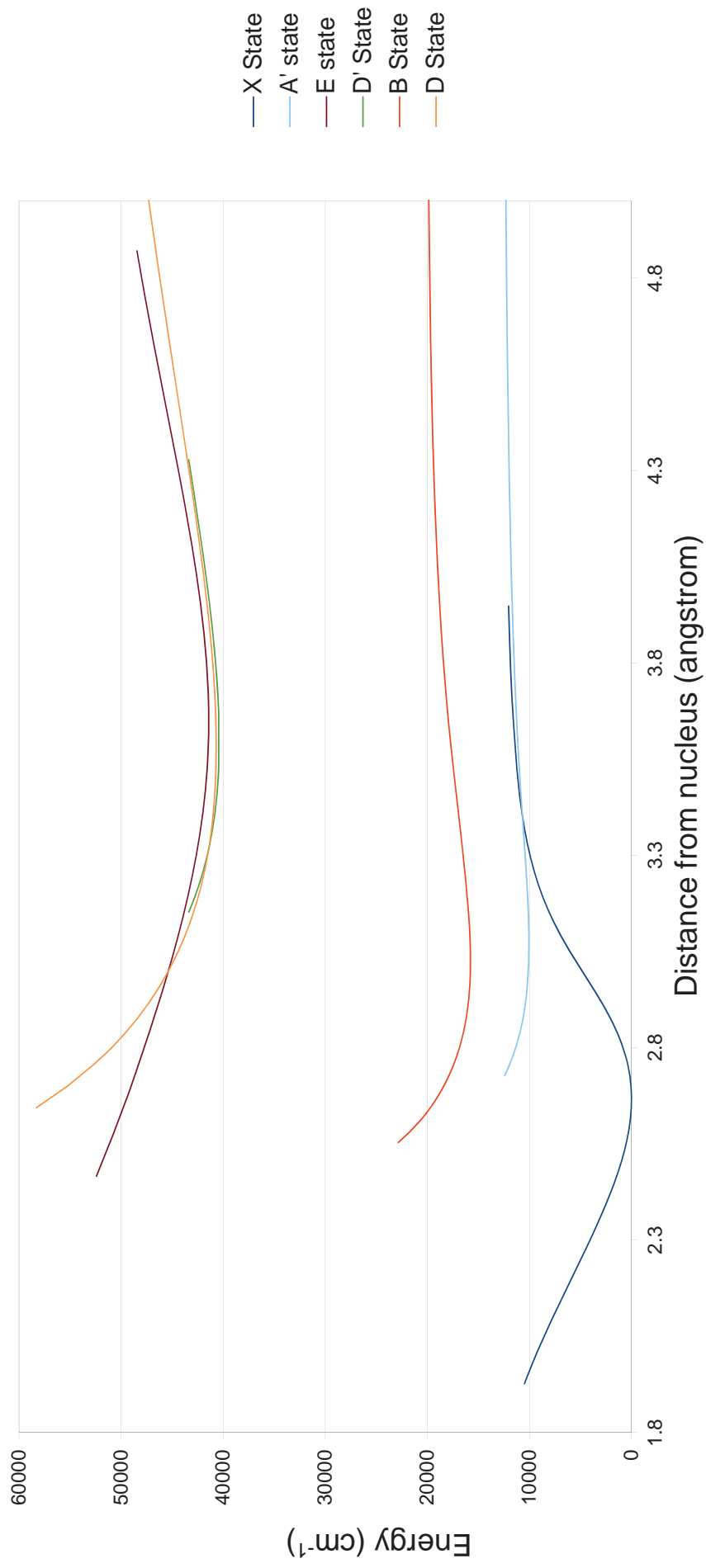
Figure 2.1: Plots of RKR curves for X, A', B, D', D, and E states.

## 2.4  Theoretical Calculations

### 2.4.1  Franck-Condon Factor Calculations

Optical excitation among molecular states is constrained by selection rules. A range of accessible vibrational states and the corresponding internuclear distances are given by the Franck-Condon principle. For vibrational transitions, the Franck-Condon requirement is $|\langle v'' \mid v' \rangle| > 0$, and for rotational transitions it is $\Delta J = 0, \pm 1$ per photon. The square of the overlap of the upper and lower vibrational wavefunctions is the Franck-Condon Factor, which determines the probability for rotational-vibrational transitions. This is accomplished by solving the radial Schrodinger equation,

$$-\frac{\hbar^2}{2\mu}\frac{d^2\Psi_{v,J}(r)}{dr^2} + V_J(r)\Psi_{v,J}(r) = E_{v,J}\Psi_{v,J}(r) \qquad (2.6)$$

where $V_J$ is the sum of the electronic potential calculated using the RKR inversion method and a centrifugal term [12, 2]. The theoretical calculations of the FCF were computed using Le Roy's program LEVEL [1]. Figures 2.2 and 2.3 map our calculated FCF values for the X-B and B-E transitions; plotted as a function of upper and lower vibrational levels. These calculations may provide predicted values for future experiments.

Figure 2.2: FCF map for vibrational levels of the X-B transitions.

Figure 2.3: FCF maps for vibrational levels of the B-E transitions.

### 2.4.2 Einstein A-Coefficient Calculations

Decay from excited levels to lower energy levels is what gives rise to spectra from molecules. When a molecule is excited to a higher level, it will spontaneously emit in the absence of a resonant electric field. The probability of decaying from a higher energy level to a lower level depends on the which lower level is being decayed to. This probability is quantified by the Einstein spontaneous emission A-coefficient, which is also termed the spontaneous emission rate. The Einstein A-coefficients for rovibronic transitions can be calculated from the transition dipole moment function, which is approximated by the equation [7, 13, 14].

$$\mu_e(R) = \sum_{i=0}^{N} \alpha_i R^i, \tag{2.7}$$

where $\alpha_i$ is experimentally determined, and R is the distance from the center of mass. Using this function, Einstein A-coefficients are calculated using the formula

$$\mathcal{A} = 3.1361891 \times 10^{-7} \frac{S(J', J'')}{2J' + 1} \nu^3 \mid \left\langle \Psi_{v',J'} \mid \mu_e(R) \mid \Psi_{v'',J''} \right\rangle \mid^2, \tag{2.8}$$

where S(J',J'') is the Honl-London rotational intensity factor, $\nu$ is the emission frequency for the transition, $\Psi_{v,J}$ are the two normalized radial wave equations, and $\mu_e$ is the transition dipole moment function [2, 7]. The theoretical calculations of the Einstein A-coefficients for the X-B and B-E transitions were computed using Le Roy's program LEVEL [1]. Figures 2.4 and 2.5 map our calculated Einstein A-coefficients for the X-B and B-E transitions; plotted as a function of upper and lower vibrational levels. These calculations may provide predicted values for future experiments.
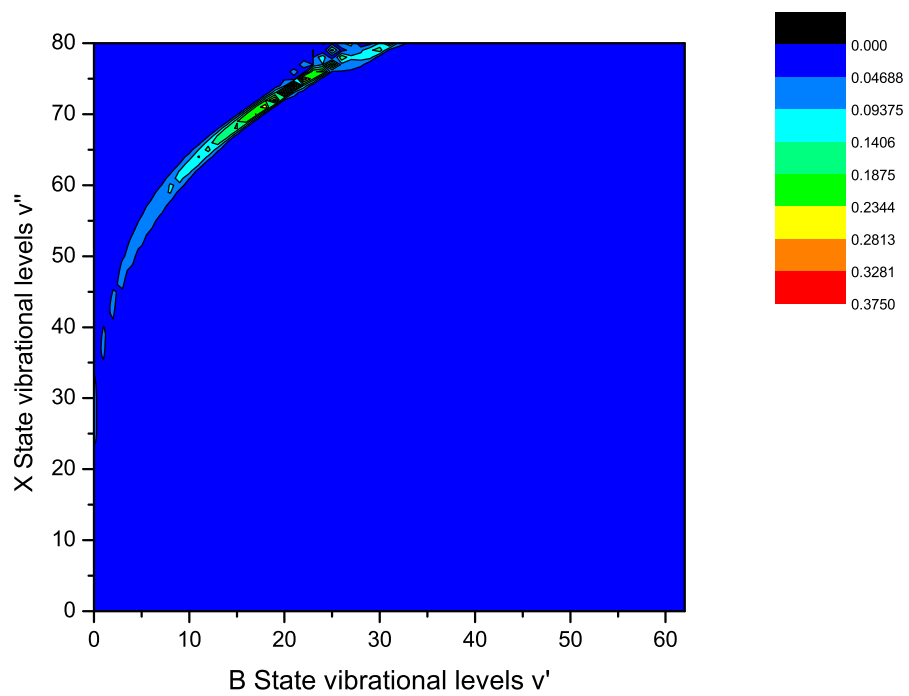
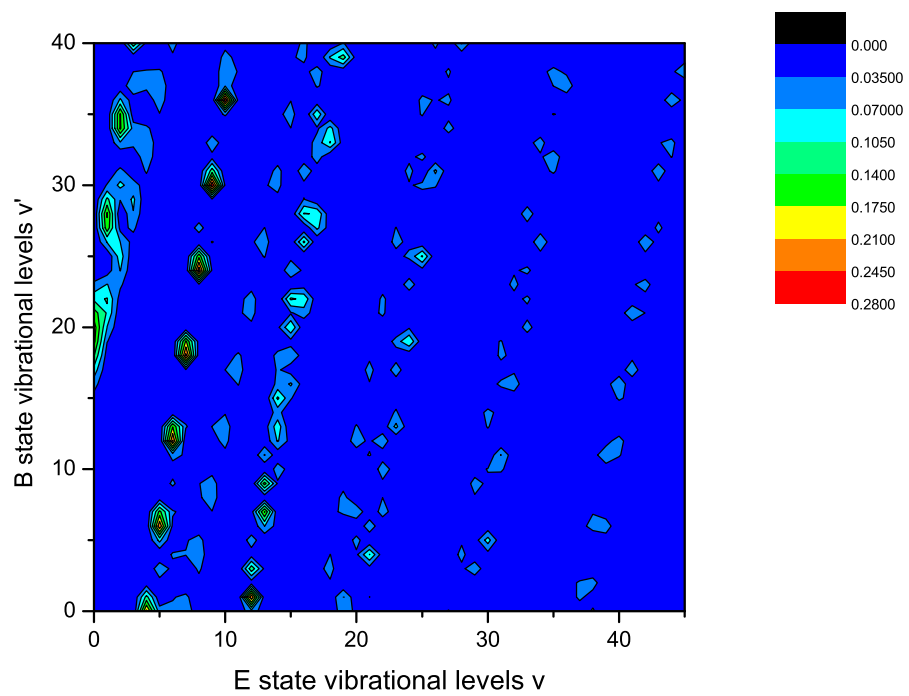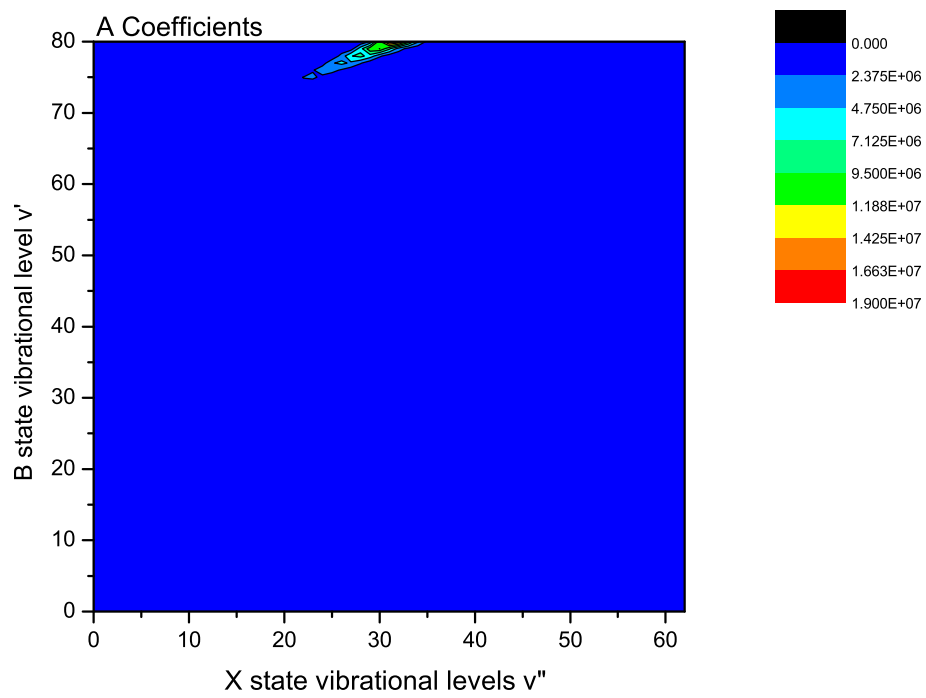Figure 2.4: Einstein A-coefficient map for vibrational levels of the X-B transitions.
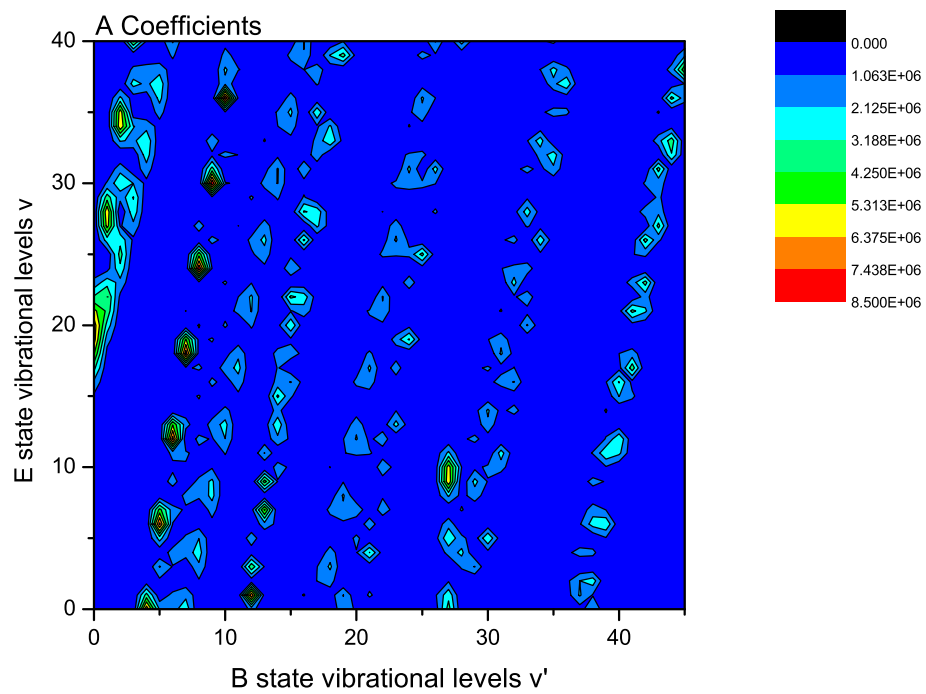
Figure 2.5: Einstein A-coefficient maps for vibrational levels of the B-E transitions.

## 2.5 Thermal Distribution of Rotational Levels

The intensity of spectral lines does not only depend on the transition probability and the frequency but also on the population of the initial state by number of molecules. In order to predict the strength of intensities, it is necessary to know the distribution of molecules in the various initial states. Since we measured our spectra in thermal equilibrium, we need to consider the thermal distribution of the molecules over different quantum states.

The thermal distribution of the rotational levels is not simply given by the Boltzmann factor $e^{(-E/kT)}$. We must also consider the degeneracy of the rotational levels; that is, the state with a total angular momentum J has a (2J+1)-fold degeneracy. Thus, the number of molecules $N_J$ in the rotational level J of the lowest vibrational state is proportional to $N_J \propto (2J+1)e^{-BJ(J+1)hc/kT}$, where B is the rotational constant. Since the factor (2J+1) increases linearly with J, the number of molecules in different rotational levels goes through a maximum. Thus, the expression for the maximum populated rotational quantum numbers J can be written as

$$J_{max} = \sqrt{kT/2Bhc} - \frac{1}{2} = 0.5896\sqrt{\frac{T}{B}} - \frac{1}{2}, \tag{2.9}$$

where T is the temperature in Kelvin and B in cm$^{-1}$ [15]. The rotational constant B for the excited electronic states of iodine is on the order of 0.02 cm$^{-1}$. The thermal distribution of rotational levels for the ground state iodine molecules is shown in Fig. 2.6. Thus, for I$_2$ at room temperature, J$_{max}$=52 in the ground X state. The rotational levels lower and higher than 52 are less populated.



Figure 2.6: Thermal distribution of the rotational levels for I$_2$ at T=300$^o$K.

## 2.6 Description of Quantum Beats

Quantum beat spectroscopy originates from a quantum interference effect of unresolved but coherently excited energy structure. Also, it is a powerful method to measure small energy differe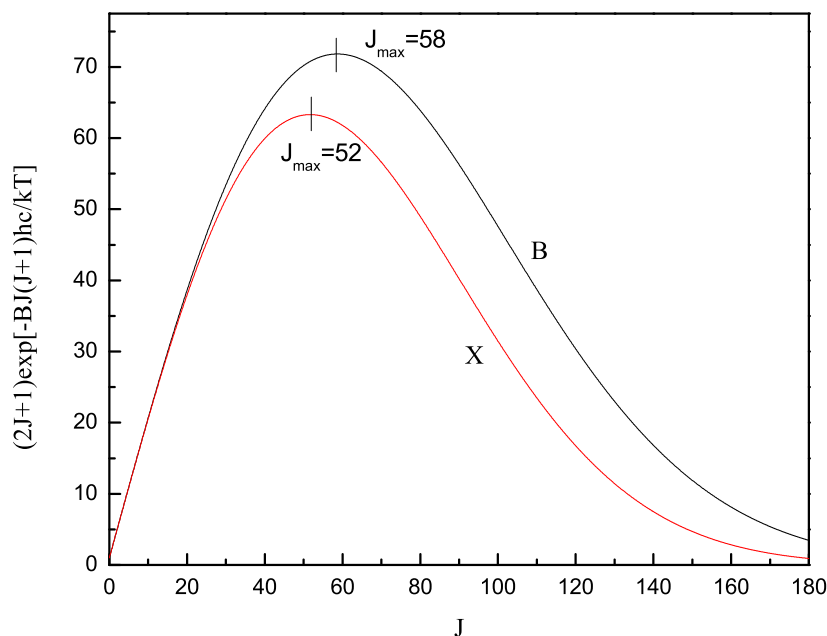nces between closely spaced levels. Quantum beat spectroscopy is not only a superior experimental technique that allows high spectral resolution measurements, but also a Doppler-free technique. A short pulse laser can create, in a molecule or an atom, a non-stationary state that may be described as a coherent superposition of stationary eigenstates. The excited superposition of states will evolve in time and results in intensity modulations of a signal at frequencies corresponding to the energy spacing between these states; this modulation is called quantum beats. The time evolution of the coherences can be directly monitored in the modulated fluorescence decay. In quantum beat spectroscopy, beats appear as oscillations superimposed on the average time-resolved fluorescence, an exponential decay. Quantum beat frequencies arising from the coherent excitation of the rotational levels within a given vibrational level are called rotational quantum beats. Rotational quantum beats exist as a result of the rotational selection rules, which state that more than one rotational level can be excited in the process. For instance, a pulsed laser can produce a coherent superposition of three rotational levels (P,Q,R branches) in the excited state of a molecule, and this can be probed by a second laser. If the coherence width of the pulse laser, determined by the time-bandwidth product for temporally Gaussian pulses ($\Delta \upsilon \sim 1/(2\Delta t)$), exceeds the small energy difference between the two excited levels, both states are coherently excited. Thus, in order to prepare coherences, the coherence width of the pulsed laser must be on the order of the splitting to be measured. If the laser bandwidth is substantially larger than the coherence width, spectral congestion problems may arise.

Quantum beat spectroscopy was originally used to determine molecular structural parameters and constants such as the Landé $g$ factor and rotational constants, or the electric dipole moments [16]. Molecular quantum beat spectroscopy has been successfully applied to polyatomic molecules [17, 18]. Also, the detection of Zeeman quantum beats has proved to be a valuable new spectroscopic tool for the measurement of Landé factors in molecular iodine in the B state [19]. In addition, quantum beat spectroscopy in potassium molecules [20] has been demonstrated and in lithium molecules using ultrafast cw-pump-probe technique has been successfully employed to study the dynamics of atomic motion [21].

# Chapter 3

# Experimental Setup and Procedure

## 3.1  Overview of the Experimental Implementation

Molecular iodine is chosen due to its spectroscopic convenience, and its accurately known spectroscopic constants [22]. In this experiment, we have applied the pump-probe technique in molecular iodine to test the feasibility of the observation of the two-photon double resonance transition for the quantum beat spectroscopy experiments. A pump transition B(v$'$=44,J$'$=41)←X(v$''$=3,J$''$=42) at 532 nm and a probe transition at 438.26 nm are selected. The selected transitions have reasonable FCFs [3, 23].

The pump laser was operated at 532 nm from the Nd:YAG second harmonic generator with FWHM bandwidth of 0.25 nm. In the first excitation step, a single rovibrational level in the B$^3\Pi_g^+$ electronic state is prepared by the pump laser. In the second step, a probe laser excites the molecules out of this state to the D$'$ state. The fluorescence spectrum was collected using a grating-variable 0.25 m spectrometer-CCD system. We used an Andor CCD operated at -45$^0$C. Energy level diagrams which demonstrate the principle of the experiment for the two-step sequence in I$_2$ is shown in Fig. 3.1. The selected transitions shown here are an example of one of the many states that we can excite by tuning the probe laser.
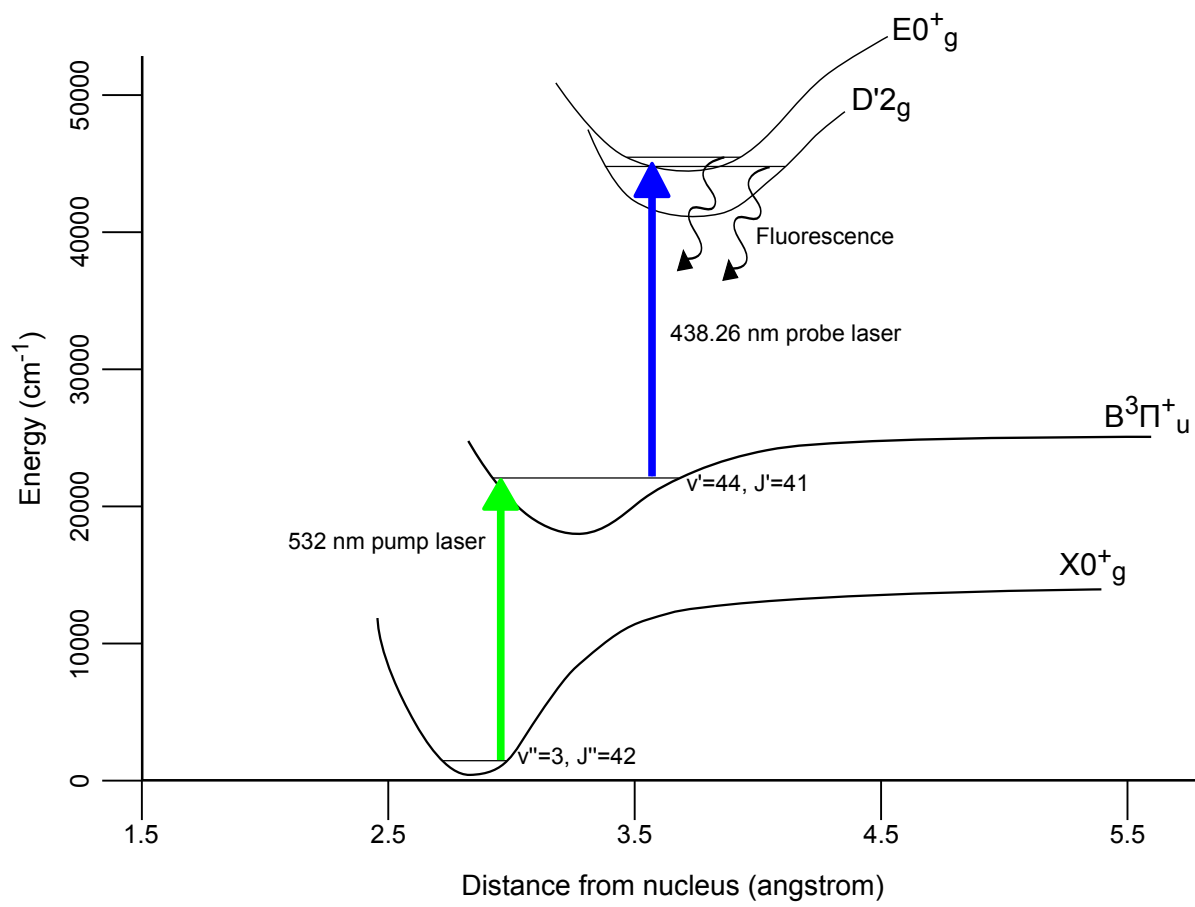
Figure 3.1: Schematic of the excitation pathway.

## 3.2 Schematic of the Experimental Apparatus

Our experimental setup can be seen in Fig. 3.2.
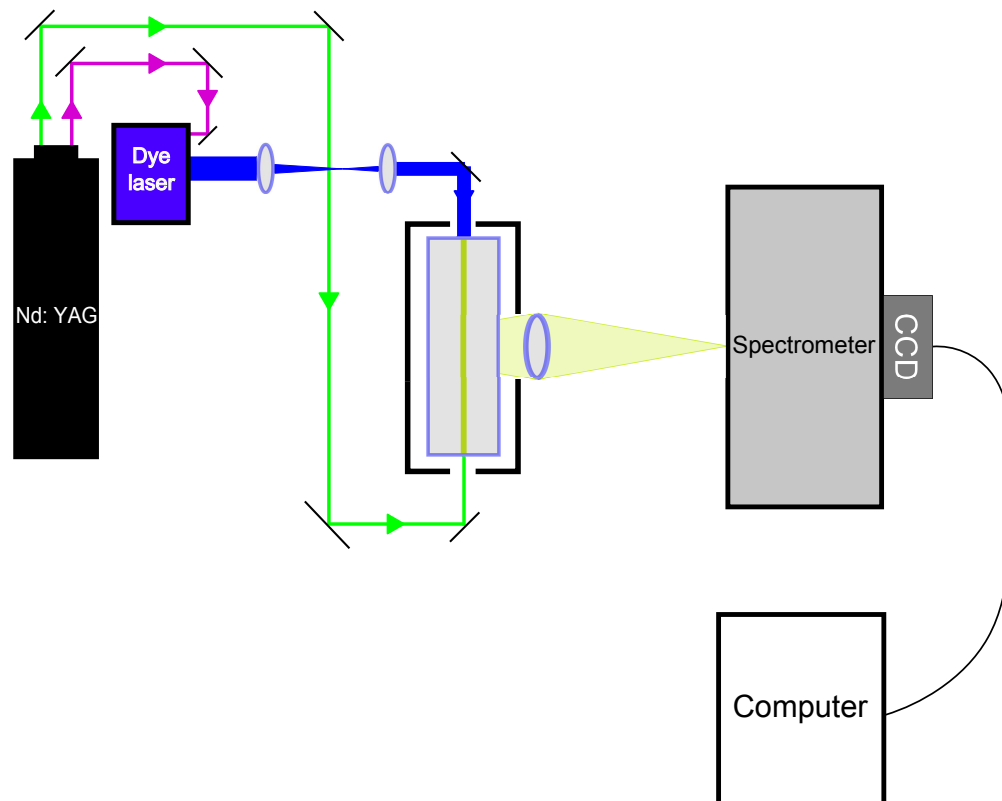


Figure 3.2: Schematic of the experimental setup.

## 3.3   Lasers

Our experiment used a pulsed pump and a tunable pulsed probe lasers. Both lasers were temporally and spatially overlapped in the iodine cell to achieve two-photon excitation. The beams were collimated to have a nearly identical cross sectional area. The fluorescence from the cell was measured on the axis perpendicular to that of the lasers, and was focused on the 25 micron slit on the spectrometer.

### 3.3.1   Pulsed Laser 1

The pump laser is generated by the second harmonic of the Nd:YAG laser. It has a peak wavelength of 532 nm, and a FWHM linewidth of 0.25 nm. The beam was collimated and attenuated before being sent through the iodine cell. The Nd:YAG laser was pulsed at 20 Hz and the pulse duration is 6 ns.

### 3.3.2   Pulsed Laser 2

The probe laser was a dye laser pumped by the third harmonic of the Nd:YAG at 355 nm and was made for the second transition (B to D$'$,E). The dye mixture had a concentration of 70.06 mg/l of Coumarin 440 (Exciton chemical company, Inc.) dissolved in methanol semiconductor grade 99.9% from Alfa Aesar. The cavity of the laser was made in the Littrow angle configuration. The cavity consisted of a 2400 lines/mm holographic grating with a high precision mount, a non-coated wedged output coupler, a quartz dye cell and a cylindrical lens. The dye cell had a dye flowing capacity and was tilted at a small angle to avoid multiple reflections arising from parallel surfaces. The dye was flowed continuously by using a micropump in order to maintain the output power. The average power was measured to be 1.2 mW. The tunability range of the blue dye laser is 430 nm - 460 nm with a peak wavelength of 443 nm. A photograph of our blue dye laser is shown in Fig. 3.3.
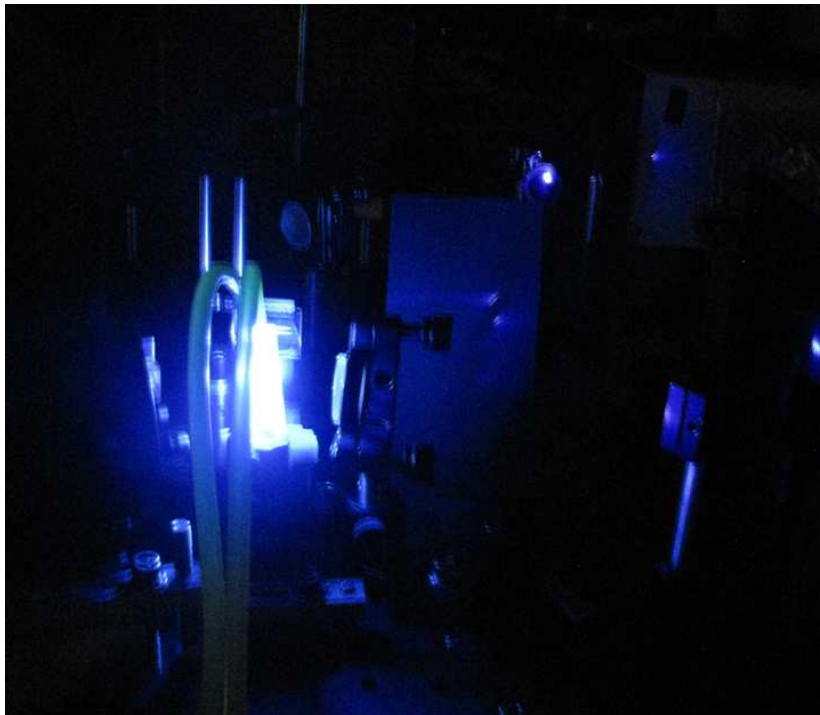
Figure 3.3: Tunable pulsed dye laser operating at 438.26 nm.

# Chapter 4

# Experimental Results and Discussion

The spectra of the single-photon pump transition and two-photon pump-probe of the B←X and D′,E←B transitions are presented. Data from both a high resolution grating (2400 lines/mm) and a medium resolution grating (600 lines/mm) are included. The wavelengths of the spectra were calibrated using well-known values for emission lines of argon and mercury gas discharge tubes. This results in resolution of 0.1 nm for the high resolution grating, and 0.3 nm for the medium resolution grating.

## 4.1   One-photon Excitation Spectrum

In the one-photon transition, a pulse pump laser at 532 nm excited B(v′=44, J′=41) ← X(v″=3, J″=42) transition. We have taken two sets of spectra: one with the medium resolution grating (600 lines/mm) and one with the high resolution grating (2400 lines/mm). We have identified ten vibrational transition peaks from the fluorescence spectrum with the medium resolution grating as shown in Fig. 4.1. Using a high resolution grating, we have resolved P, Q and R rotational branches for the two vibrational peaks as shown in Fig. 4.2.
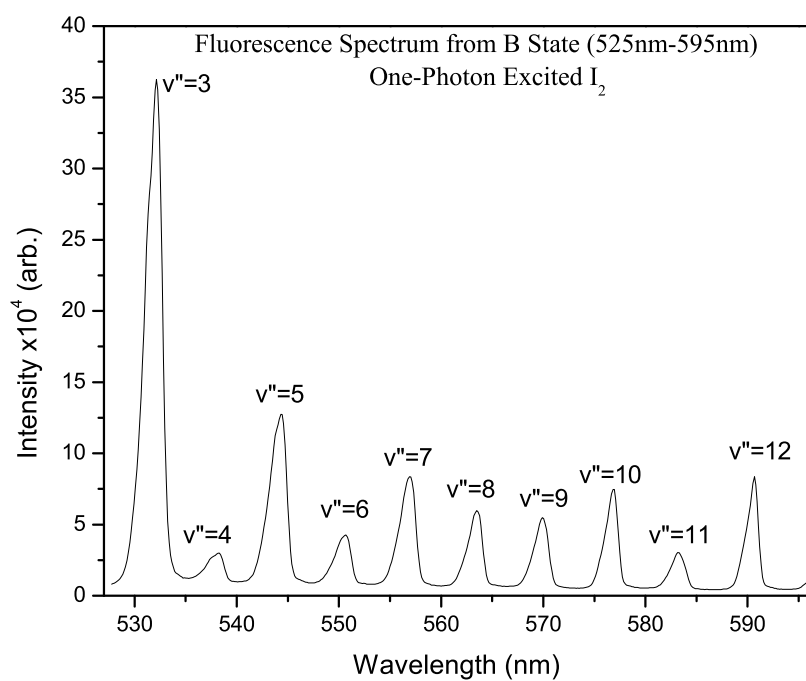
Figure 4.1: Ten vibrational peaks are identified with a 0.3 nm resolution grating.
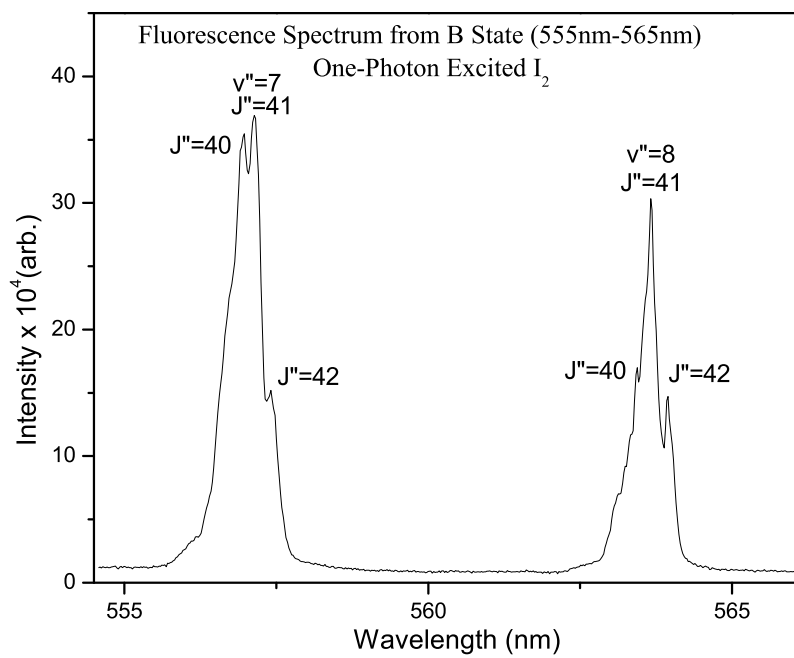
Figure 4.2: P,Q and R rotational peaks are identified using a 0.1 nm resolution grating.

## 4.2   Two-photon Excitation Spectrum

Based on the accurate molecular constants [24, 5, 1, 25] for the B-X system, the intermediate B(v′,J′) states excited by the fixed 532 nm output could be identified. Thus, the B-D′ and B-E excitation could be inferred. Figures 4.3 to 4.6 show all observed peaks for the two-photon pump-probe $E0_g^+ \leftarrow B^3\Pi_u^+ \leftarrow X0_g^+$ and $D'2_g \leftarrow B^3\Pi_u^+ \leftarrow X0_g^+$ transitions. Analysis of the peaks observed will be presented in the next section.
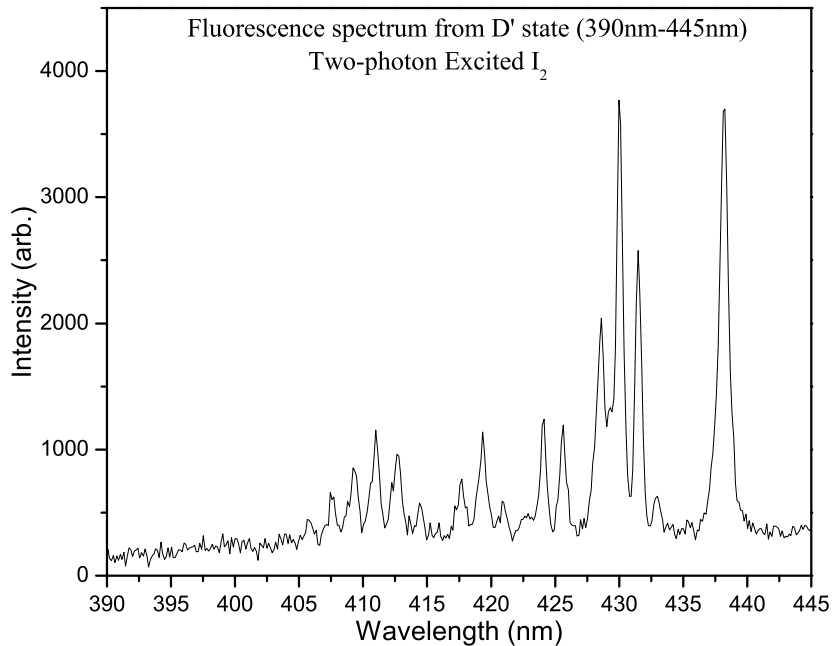


Figure 4.3: Entire observed two-photon spectrum.
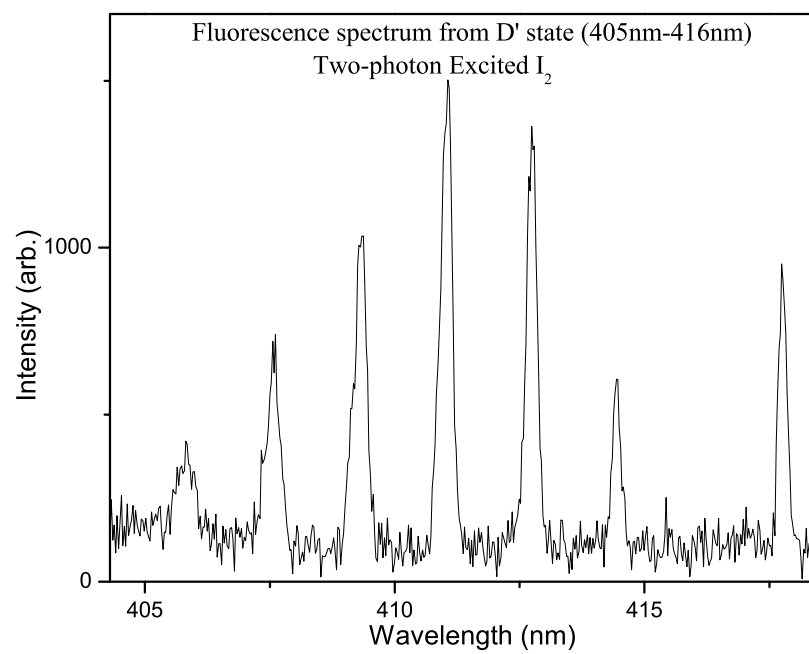
Figure 4.4: Seven peaks of the 405-416 nm range of the two-photon spectrum.
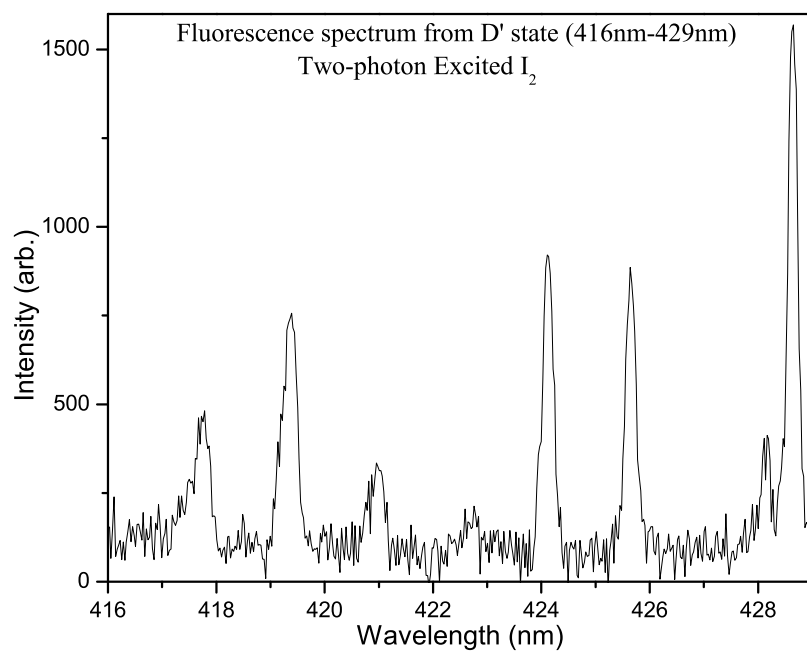
Figure 4.5: Eight peaks of the 416-429 nm range of the two-photon spectrum.
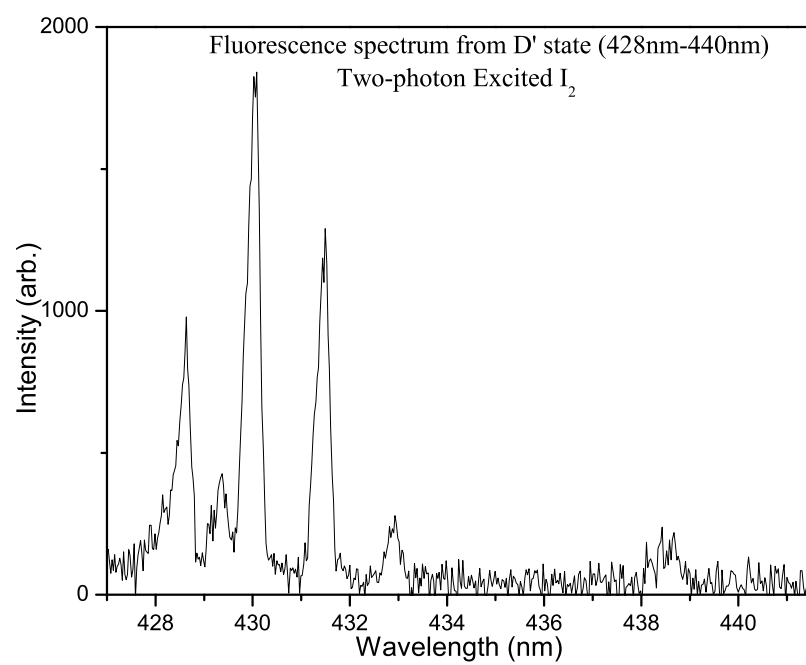
Figure 4.6: Five peaks of the 428-440 nm range of the two-photon spectrum.

## 4.3 Discussion

Table 4.1 demonstrates agreement between observed peak wavelengths and theoretical calculated wavelengths. The regularly spaced peaks seen in Fig. 4.1 are clearly emission from B(v'=44,J'=41) to the given vibrational levels of the X ground state. The P, Q, and R rotational lines are also visible in Fig. 4.2, and Table 4.2 shows agreement between observed and theoretical peak wavelengths. The FCF for the first transition is comparatively low, with a value of only $6.36\times10^{-4}$. However, due to the high intensity of the pump laser, this transition is still easily excited, as seen by the strong peak in Fig. 4.1. Additionally, our high resolution spectrum seen in Fig. 4.2 shows three rotational peaks for each vibrational peak. This strongly suggests that the first transition made by the pump laser is only B(v'=44,J'=41)← X(v''=3,J''=42) and no other rovibrational transitions exist. If multiple transitions were being made, more peaks would appear clustered around the vibrational peaks. For example: if the two adjacent rotational levels B(v'=44,J'=41,42) were excited by X(v''=3,J''=42), one would observe four peaks: the P, Q, and R branches from each of the two rotational levels, two of which are the same transition. Since only three rotational lines are observed for each vibrational line, either a single transition is being made, or we cannot resolve the closely-lying peaks. Due to the sensitivity of our spectrometer-CCD setup and the varying FCFs of the transitions, we rule the latter case out as unlikely.

Identifying the second transition is considerably more difficult for several reasons. Although a spectrum is clearly observed, the peaks shown in Fig. 4.3 do not appear as an evenly-spaced set of peaks with decreasing intensity, as was the case for the first transition. This is a consequence of the fact that the D' and E electronic states are very close in energy, as can be seen in Fig. 2.1. Also, these states have more electronic states to decay to than the B state, which further increases the number of closely-grouped peaks that will occur in the fluorescence. Intensity of the observed peaks from the two-photon fluorescence was also significantly less than that from the first transition, which may have caused some emission peaks to be lost in the signal noise from ambient light. However, as Table 4.3 shows, there are many transitions whose theoretical emission wavelengths agree with the observed peak wavelengths. A more accurate spectrum obtained from a higher-resolution spectrometer and better calibration source would allow for more conclusive peak identification. Regardless, the two-photon spectrum obtained demonstrates that a two-step optical pathway is indeed being excited in iodine with our system.

Although mercury and argon emission tubes were used to calibrate data, conveniently-spaced emission lines were not always available at the wavelength we were observing, which caused our calibrations to be less accurate. Due to the high sensitivity of our CCD, ambient light leaks may have obscured some of the lower-intensity peaks in the two-photon spectrum. Although some power broadening of the lines likely occurred, the clearly-resolved rotational lines show that this is not a concern for the first transition. Although not tested experimentally, power and Doppler broadening may have obscured rotational lines in the two-photon spectra, as only single peaks were observed with the high resolution grating. However, since the two lasers used were counter-propagating, Doppler broadening was minimized.

Tables 4.1 and 4.2 correspond to the peaks observed and spectra presented in Figures 4.1 and 4.2, respectively.

Table 4.1: Experimental and Theoretical Values for One-Photon Vibrational Peaks

| Experimental (nm) | Theoretical (nm) | Possible Transition from B(44,41) to X(v″,J″) | Error (nm) |
|---|---|---|---|
| 532.1392 | 532.1364 | (3,42) | 0.0028 |
| 538.3060 | 538.0483 | (4,41) | 0.2577 |
| 544.3076 | 544.1498 | (5,41) | 0.1579 |
| 550.6878 | 550.3531 | (6,41) | 0.3347 |
| 556.9015 | 556.6602 | (7,41) | 0.2413 |
| 563.4871 | 563.0731 | (8,41) | 0.4140 |
| 569.9049 | 569.5937 | (9,41) | 0.3111 |
| 576.8201 | 576.2241 | (10,41) | 0.5961 |
| 583.1690 | 582.9662 | (11,41) | 0.2028 |
| 590.6654 | 589.8222 | (12,41) | 0.8432 |
|  |  | Average Error: | 0.3362 |

Table 4.2: Experimental and Theoretical Values for One-Photon Rovibrational Peaks

| Experimental (nm) | Theoretical (nm) | Possible Transition from B(44,41) to X(v″,J″) | Error (nm) |
|---|---|---|---|
| 556.9756 | 556.5631 | (7,40) | 0.4124 |
| 557.1359 | 556.6602 | (7,41) | 0.4757 |
| 557.4105 | 556.7597 | (7,42) | 0.6509 |
| 563.4398 | 562.9735 | (8,40) | 0.4663 |
| 563.6609 | 563.0731 | (8,41) | 0.5878 |
| 563.9480 | 563.1752 | (8,42) | 0.7728 |
|  |  | Average Error: | 0.5610 |

Table 4.3: Experimental and Theoretical Values for Likely Two-Photon Emission Peaks

| Exp. (nm) | Theory D′ (nm) | Possible transition D′(v,J)-B(v′,J′) | Theory E (nm) | Possible transition E(v,J)-B(v′,J′) | Error in D′ (nm) | Error in E (nm) |
|---|---|---|---|---|---|---|
| 405.6458 | 405.2377 | (20,40)-(17,42) | 406.3165 | (9,40)-(17,39) | 0.4081 | 0.6707 |
| 407.4311 | 406.6962 | (20,40)-(18,39) | 407.8887 | (9,40)-(18,39) | 0.7349 | 0.4576 |
| 409.2151 | 409.7626 | (20,40)-(17,42) | 409.4413 | (9,40)-(19,39) | 0.5475 | 0.2261 |
| 410.9979 | 411.3327 | (20,40)-(20,39) | 410.9878 | (9,42)-(20,41) | 0.3348 | 0.0101 |
| 412.6424 | 412.74315 | (20,40)-(22,39) | 412.5526 | (9,40)-(21,41) | 0.1008 | 0.08982 |
| 414.4227 | 414.3093 | (20,42)-(23,43) | 413.9714 | (9,40)-(22,39) | 0.1134 | 0.4513 |
| 417.7060 | 417.1455 | (20,42)-(25,43) | 417.9836 | (10,42)-(26,41) | 0.5605 | 0.2776 |
| 419.3461 | 419.7693 | (20,40)-(27,39) | 419.3556 | (10,40)-(27,40) | 0.4232 | 0.0096 |
| 420.8485 | 421.0944 | (20,40)-(28,39) | 420.7248 | (10,42)-(28,43)) | 0.24591 | 0.1237 |
| 422.8958 | 422.4268 | (20,42)-(29,41) | 422.4535 | (9,42)-(28,43) | 0.4690 | 0.4423 |
| 424.1234 | 423.7628 | (20,42)-(30,43) | 424.4366 | (10,40)-(31,39) | 0.3606 | 0.31327 |
| 425.6229 | 426.1002 | (20,40)-(32,39) | 425.6398 | (10,40)-(32,39) | 0.4773 | 0.0169 |
| 428.6192 | 428.5173 | (20,42)-(34,43) | 428.6231 | (9,40)-(33,40) | 0.1019 | 0.00394 |
| 429.980 | 429.6257 | (20,42)-(25,43) | 429.8135 | (9,42)-(34,43) | 0.35428 | 0.1664 |
| 430.0814 | 429.6257 | (20,42)-(35,43) | 430.1321 | (10,40)-(36,39) | 0.4557 | 0.05073 |
| 431.4759 | 431.6452 | (20,40)-(37,39) | 431.2358 | (10,40)-(37,41) | 0.1693 | 0.2400 |
| 432.9709 | 432.75104 | (20,42)-(38,43) | 432.9888 | (9,40)-(37,39) | 0.2199 | 0.0179 |
| | | | | Average Error: | 0.3575 | 0.2099 |

# Chapter 5

# Future Developments

We have demonstrated that our system can be used to excite a two-step optical pathway in $I_2$. Future improvements to our setup include using a narrow bandwidth laser to excite the $B^3\Pi_u^+$ ($v'$=44, $J'$=41) $\leftarrow$ $X0_g^+$ ($v''$=3,$J''$=42) optical pathway to avoid spectral congestion and using a pulsed, tunable, sufficiently broadband probe laser to coherently excite three rotational levels in the $D'2_g$ state to observe quantum beats. Using quantum beat spectroscopy and a 1.5 m spectrometer-CCD/PMT setup, precise, high resolution spectra can be obtained. This data may then be used to determine Dunham coefficients, electric dipole moment transition functions, and to provide more accurate spectra of $I_2$ for calibration and future study.

# Bibliography

[1] R. J. LeRoy. *J. Chem. Phys.*, 52:2683, 1970.

[2] R. J. Le Roy. A computer program for solving the radial schrodinger equation for bound and quasibound levels. Technical report, U. of Waterloo, 2007.

[3] T. Ishiwata and I. Tanaka. *Laser Chem.*, 7:79, 1987.

[4] D. Cerny, R. Bacis, S. Churassy, D. Inard, M. Lamrini, and M. Nota. *Chem. Phys.*, 216:207, 1997.

[5] J. C. D. Brand, A. R. Hoy, A. K. Kalkar, and A. B. Yamashita. *J. Mol. Spec.*, 95:350, 1982.

[6] S. Wilson. *Handbook of Molecular Physics and Quantum Chemistry*. John Wiley  Sons, Ltd., 2002.

[7] H. L. Lefebvre-Brion and R. W. Field. *The Spectra and Dynamics of Diatomic Molecules*. Elsevier Academic Press, 2004.

[8] J. L. Dunham. The energy levels of a vibrating rotator. *Phys. Rev.*, 41:721, 1932.

[9] R. Rydberg. *Z. Physik*, 73:376, 1931.

[10] R. Rydberg. *Z. Physik*, 80:514, 1933.

[11] O. Klein. *Z. Physik*, 76:226, 1932.

[12] R. N. Zare. *J. Chem. Phys.*, 40:1934, 1964.

[13] G. L. Bhale, S. F. Ahmad, and S. P. Reddy. *J. Phys. B: Atm. Mol. Phys.*, 18:645, 1985.

[14] M. E. Akopyan, V. V. Baturo, S. S. Lukashov, S. A. Poretsky, and A. M. Pravilov. *J. Phys. B*, 133:244304, 2011.

[15] G. Herzberg. *Molecular Spectra and Molecular Structure-I. Spectra of Diatomic Molecules*. D. Van Nostrand Company, New York, 1950.

[16] P. M. Felker and A. H. Zewail. *Advances in Chemical Physics*. Wiley, 1988.

[17] H. Bitto and J. R. Huber. *Optics Comm.*, 80:184, 1990.

[18] J. Velazquez, N. Hemmi, and T. A. Cool. *Chem. Phys. Lett.*, 221:39, 1994.

[19] R. Wallenstein, J. A. Paisner, and A. L. Schawlow. *Phys. Rev. Lett.*, 32:1333, 1974.

[20] M. P. Auzin'sh and R. S. Ferber. *JETP Lett.*, 39:452, 1984.

[21] J. M. Papanikolas, R. M. Williams, P. D. Kleiber, J. L. Hart, C. Brink, S. D. Price, and S. R. Leone. *J. Chem. Phys.*, 103:7269, 1995.

[22] A. A. Radzig and B. M. Smirnov. *Reference Data on Atoms, Molecules, and Ions.* Springer-Verlag, New York, 1985.

[23] M. Allegrini, G. Alzetta, and M. Civilini. *Chem. Phys. Lett.*, 70:454, 1980.

[24] J. I. Steinfeld, R. N. Zare, L. Jones, M. Lesk, and W. Klemperer. *J. Chem. Phys.*, 42:25, 1965.

[25] J. D. Brown, G. Burns, and R. J. LeRoy. *Can. J. Phys.*, 51(15):1664, 1973.

# Chapter 6

# Appendix

## 6.1 Tables of Dunham Coefficients

The following tables show the Dunham coefficients of iodine molecules in the X,B,D and E states that were used.

Table 6.1: Dunham coefficients $Y_{n,k}$ for the X state [1].

| $Y_{n,k}$ | n=0 | n=1 | n=2 | n=3 | n=4 |
|---|---|---|---|---|---|
| k=0 | 0 | $2.15\times10^2$ | $-6.16\times10^{-1}$ | $7.51\times10^{-5}$ | $-1.26\times10^{-4}$ |
| k=1 | $3.74\times10^{-2}$ | $-1.24\times10^{-4}$ | $4.50\times10^{-7}$ | $-1.48\times10^{-8}$ | $-3.64\times10^{-11}$ |
| k=2 | $4.54\times10^{-9}$ | $1.70\times10^{-11}$ | $7.00\times10^{-12}$ | | |

Table 6.2: Dunham coefficients $Y_{n,k}$ for the B state [2].

| $Y_{n,k}$ | n=0 | n=1 | n=2 | n=3 | n=4 |
|---|---|---|---|---|---|
| k=0 | 15768.947 | $1.26\times10^2$ | $-7.48E\times10^{-1}$ | $-5.02\times10^{-3}$ | $3.79\times10^{-4}$ |
| k=1 | $2.90\times10^{-2}$ | $-1.50\times10^{-4}$ | $-1.12\times10^{-6}$ | $-8.60\times10^{-9}$ | $-3.99\times10^{-9}$ |
| k=2 | $5.40\times10^{-9}$ | $-3.00\times10^{-10}$ | | | |

Table 6.3: Dunham coefficients $Y_{n,k}$ for the D state [3].

| $Y_{n,k}$ | n=0 | n=1 | n=2 | n=3 | n=4 |
|---|---|---|---|---|---|
| k=0 | 41028.584 | $9.50\times10^1$ | $-1.09\times10^{-1}$ | $-5.81\times10^{-4}$ | $3.69\times10^{-6}$ |
| k=1 | $2.07\times10^{-2}$ | $-4.37\times10^{-5}$ | $-8.99\times10^{-8}$ | $6.58\times10^{-10}$ | |
| k=2 | $-4.93\times10^{-9}$ | | | | |

Table 6.4: Dunham coefficients $Y_{n,k}$ for the D$'$ state [4].

| $Y_{n,k}$ | n=0 | n=1 | n=2 | n=3 | n=4 |
|---|---|---|---|---|---|
| k=0 | $4.04\times10^4$ | $1.03\times10^2$ | $1.86\times10^{-1}$ | $-6.61\times10^{-2}$ | $6.03\times10^{-4}$ |
| k=1 | $1.32\times10^{-2}$ | $4.91\times10^{-3}$ | $-1.35\times10^{-3}$ | $1.92\times10^{-4}$ | $-1.49\times10^{-5}$ |

Table 6.5: Dunham coefficients $Y_{n,k}$ for the E state [5].

| $Y_{n,k}$ | n=0 | n=1 | n=2 | n=3 | n=4 |
|---|---|---|---|---|---|
| k=0 | 41411.764 | $1.01\times10^2$ | $-2.05\times10^{-1}$ | $5.71\times10^{-4}$ | $-1.19\times10^{-5}$ |
| k=1 | $2.00\times10^{-2}$ | $-5.45\times10^{-5}$ | $2.38\times10^{-8}$ | $1.13\times10^{-10}$ | |
| k=2 | $-3.25\times10^{-9}$ | $1.16\times10^{-11}$ | | | |

## 6.2 Tables of Transition Dipole Function Coefficents

The following tables show the electric dipole moment transition function coefficients used for the B-X and D$'$-B transitions [13, 14].

Table 6.6: Transition Dipole Moment Function Coefficients

| | B-X | E-B |
|---|---|---|
| $\alpha_0$ | -500.358 | 15.97 |
| $\alpha_1$ | 377.125 | -3.31 |
| $\alpha_2$ | -38.483 | -1.08 |
| $\alpha_3$ | -25.429 | -0.30 |
| $\alpha_4$ | 4.9831 | -0.03 |
| $\alpha_5$ | | 0.037 |
| $\alpha_5$ | | 0.0310 |
| $\alpha_5$ | | 0.00702 |
| $\alpha_5$ | | -0.0076 |
| $\alpha_5$ | | 0.001 |

## 6.3 RKR1 and LEVEL8.0 Input Files

The following is a sample input file for RKR1.

```
53 127 53 127 0 0 0
Dunham Calculation for I2(B)
16
1.256643430002D+2 -7.475284960242D-01 -5.016833169864D-3 3.788414181699D-4
-4.983773834286D-5 4.200565944860D-06 -2.462699605029D-7 1.035559345644D-8
-3.168784847369D-10 7.099055257498D-12 -1.159685360751D-13 1.361205680478D-15
-1.115309496593D-17 6.046170833273D-20 -1.947198245975D-22 2.820031243526D-25
15
2.900080684844D-2 -1.496203558218D-04 -1.122999681016D-6 -8.598750387065D-9
-3.993514191186D-9 7.442705931721D-10 -7.729114740147D-11 4.998660579762D-12
-2.157393379080D-13 6.436910217056D-15 -1.347501253707D-16 1.977227945639D-18
-1.994896518940D-20 1.320031684314D-22 -5.162433698190D-25 9.047632057664D-28
```

0 2 45.d0
-0.4d0 0.2d0 1.6d0
2.0d0 1.0d0 82.d0

     The following is a sample input file for LEVEL 8.0
53 127 53 127 0 2
'Predict emission for B-X I2'
0.0015 1.85 15.0 1.d-4
124 0 0 20150.0d0
10 0 1 0 0.D0
1.D0 1.D0 15768.947d0
2.653997278 4016.1322855685 2.6543895536 3984.2245292402
2.6549011316 3950.5452124362 2.6555314613 3915.0550558141
2.6562803502 3877.7164111245 2.6571479502 3838.4934939459
2.6581347453 3797.3526139989 2.6592415421 3754.2623947494
2.6604694592 3709.193974627 2.6618199163 3662.121183146
2.6632946226 3613.0206864486 2.6648955657 3561.8720982182
2.6666250011 3508.6580534407 2.6684854454 3453.3642440458
———————-other values omitted———————
5.5870088507 4230.6147520079 5.6935592513 4247.1933069676
5.8069391548 4262.49282694 5.9278914505 4276.5620808196
6.0572696882 4289.4506604897 6.1960578668 4301.2090443233
6.3453947481 4311.8886389234 6.5066040856 4321.5417888793
6.6812326796 4330.2217459045 6.8710989286 4337.9825906763
7.078355655 4344.8791034385 7.3055726408 4350.966582397
134 0 0 12530.0D0
10 0 0 6 0.D0
1.D0 1.D0 0.d0
1.8561738498 11122.7151100858 1.8688811463 11005.8614820475
1.8813202992 10884.1238352388 1.8935200281 10757.5743766664
1.9055075212 10626.2932581246 1.9173084302 10490.3669438813
1.9289468869 10349.8866891139 1.9404455364 10204.9471456728
1.951825584 10055.6451060418 1.9631068515 9902.0783913737
———————-other values omitted———————
3.7701014508 11948.8694500128 3.8159852205 12015.8805196772
3.8652771395 12078.2041623996 3.9182909481 12135.9734422292
3.9753759457 12189.3375653961 4.0369297212 12238.458083647
4.1034206467 12283.5036679622 4.1754274417 12324.6432156512
4.2537083386 12362.0370300346 4.3393218131 12395.8257867348
4.4338390574 12426.1169739571 4.5397268718 12452.96846603
4.6610698625 12476.3688598345 4.8050384119 12496.2141725593
4.9852287087 12512.2804664239 5.2306326156 12524.1919315894
-40 1 0 -4 130 1 -1 0
0 0
4 0 1.D0
-500.358 377.125 -38.483 -25.429 4.9831
15 1 -1 +1 2
0 1 2 3 4 5 6 7 8 9 10 11 12 13 14

## 6.4 Sample Output Files

The following is a typical sample output file from LEVEL 8.0
Predict emission for B-X I2
================================================================
Note that (v′,J′) (v",J") strictly label the upper and lower levels, resp.,
and E(lower)=E"
but E(2)-E(1) is: (energy of State-2 level) - (energy of State-1 level)

Band
$\Delta$J(J") v′ v" E(lower) E(2)-E(1) A(Einstein) F-C Factor <v′j′|M|v"j"¿
—— ——- —— ——— ——— ——— ———

P( 1) 0 - 0 107.07 -15724.4926 1.89404D-03 4.10351D-10 3.94120D-05
P( 1) 0 - 1 320.39 -15511.1790 2.90672D-02 6.51461D-09 1.57592D-04
P( 1) 0 - 2 532.46 -15299.1013 2.28803D-01 5.32062D-08 4.51368D-04
P( 1) 0 - 3 743.30 -15088.2634 1.23190D+00 2.98052D-07 1.06937D-03
P( 1) 0 - 4 952.90 -14878.6710 5.10413D+00 1.28815D-06 2.22287D-03
P( 1) 0 - 5 1161.24 -14670.3311 1.73585D+01 4.58050D-06 4.18693D-03
P( 1) 0 - 6 1368.31 -14463.2515 5.04690D+01 1.39549D-05 7.29311D-03
P( 1) 0 - 7 1574.13 -14257.4408 1.29004D+02 3.74529D-05 1.19135D-02
P( 1) 0 - 8 1778.66 -14052.9081 2.95855D+02 9.03560D-05 1.84369D-02
P( 1) 0 - 9 1981.90 -13849.6628 6.18225D+02 1.98964D-04 2.72404D-02
P( 1) 0 - 10 2183.85 -13647.7147 1.19131D+03 4.04672D-04 3.86564D-02
P( 1) 0 - 11 2384.49 -13447.0738 2.13739D+03 7.67474D-04 5.29419D-02
P( 1) 0 - 12 2583.82 -13247.7505 3.59841D+03 1.36772D-03 7.02491D-02
P( 1) 0 - 13 2781.81 -13049.7554 5.72127D+03 2.30492D-03 9.06028D-02
P( 1) 0 - 14 2978.47 -12853.0992 8.63684D+03 3.69253D-03 1.13884D-01
P( 1) 1 - 0 107.07 -15848.6469 3.12847D-02 6.64590D-09 -1.58299D-04
P( 1) 1 - 1 320.39 -15635.3333 4.49426D-01 9.85730D-08 -6.12304D-04
P( 1) 1 - 2 532.46 -15423.2556 3.30301D+00 7.50302D-07 -1.69430D-03
————————————-Other values omitted————————————
P( 1) 44 - 10 2183.85 -17400.0316 2.43357D+04 4.35626D-03 1.21366D-01
P( 1) 44 - 11 2384.49 -17199.3908 2.73776D+02 2.49042D-05 1.30987D-02
P( 1) 44 - 12 2583.82 -17000.0675 1.70430D+04 3.25656D-03 -1.05171D-01
P( 1) 44 - 13 2781.81 -16802.0723 1.97513D+04 3.56023D-03 -1.15227D-01
P( 1) 44 - 14 2978.47 -16605.4161 3.49036D+02 4.17715D-05 -1.55905D-02
P( 1) 45 - 0 107.07 -19517.1750 5.17244D+04 1.13689D-02 -1.48943D-01
P( 1) 45 - 1 320.39 -19303.8615 3.60170D+02 5.77664D-05 1.26353D-02
P( 1) 45 - 2 532.46 -19091.7837 3.43532D+04 7.10898D-03 1.25462D-01
P( 1) 45 - 3 743.30 -18880.9458 1.48140D+03 3.18416D-04 2.64911D-02
P( 1) 45 - 4 952.90 -18671.3535 2.58208D+04 5.10254D-03 -1.12466D-01
P( 1) 45 - 5 1161.24 -18463.0136 1.38153D+04 2.65638D-03 -8.36613D-02
P( 1) 45 - 6 1368.31 -18255.9340 7.78733D+03 1.54279D-03 6.38833D-02
P( 1) 45 - 7 1574.13 -18050.1233 2.90819D+04 5.44836D-03 1.25571D-01
P( 1) 45 - 8 1778.66 -17845.5905 1.23261D+03 1.84663D-04 2.62975D-02

P( 1) 45 - 9 1981.90 -17642.3452 1.85442D+04 3.55203D-03 -1.03769D-01
P( 1) 45 - 10 2183.85 -17440.3971 2.06147D+04 3.66358D-03 -1.11315D-01
P( 1) 45 - 11 2384.49 -17239.7562 2.40792D+01 1.73882D-05 3.87100D-03
P( 1) 45 - 12 2583.82 -17040.4329 1.92526D+04 3.63887D-03 1.11384D-01
P( 1) 45 - 13 2781.81 -16842.4378 1.60392D+04 2.85064D-03 1.03462D-01
P( 1) 45 - 14 2978.47 -16645.7816 1.92285D+01 1.26925D-05 -3.64599D-03